International Journal of Mechanical, Industrial and Aerospace Sciences
ISSN: 2517-9950
Vol:8, No:4, 2014

LIDAR Obstacle Warning and Avoidance System for Unmanned Aircraft

Roberto Sabatini, Alessandro Gardi, Mark A. Richardson

***Abstract*—**The availability of powerful eye-safe laser sources and the recent advancements in electro-optical and mechanical beam-steering components have allowed laser-based Light Detection and Ranging (LIDAR) to become a promising technology for obstacle warning and avoidance in a variety of manned and unmanned aircraft applications. LIDAR outstanding angular resolution and accuracy characteristics are coupled to its good detection performance in a wide range of incidence angles and weather conditions, providing an ideal obstacle avoidance solution, which is especially attractive in low-level flying platforms such as helicopters and small-to-medium size Unmanned Aircraft (UA). The Laser Obstacle Avoidance Marconi (LOAM) system is one of such systems, which was jointly developed and tested by SELEX-ES and the Italian Air Force Research and Flight Test Centre. The system was originally conceived for military rotorcraft platforms and, in this paper, we briefly review the previous work and discuss in more details some of the key development activities required for integration of LOAM on UA platforms. The main hardware and software design features of this LOAM variant are presented, including a brief description of the system interfaces and sensor characteristics, together with the system performance models and data processing algorithms for obstacle detection, classification and avoidance. In particular, the paper focuses on the algorithm proposed for optimal avoidance trajectory generation in UA applications.

***Keywords*—**LIDAR, Low-Level Flight, Nap-of-the-Earth Flight, Near Infra-Red, Obstacle Avoidance, Obstacle Detection, Obstacle Warning System, Sense and Avoid, Trajectory Optimisation, Unmanned Aircraft.

I. Introduction

LOW level navigation and terrain-following operations with UA are challenged by a variety of natural and man-made obstacles, as well as by adverse weather conditions that can significantly reduce the obstacles visibility. Reduced visibility is the main factor preventing the UA pilot from safely controlling the aircraft and from identifying possible obstacle collision hazards. In these scenarios, radar has been traditionally employed to automatically maintain a safe separation from the ground by flying the aircraft at a certain altitude above the terrain. However, state-of-the-art avionics radars lack sufficient angular resolution to be able to detect small natural and man-made obstacles such as trees, power line cables and poles. The outstanding angular resolution and accuracy characteristics of Light Detection and Ranging (LIDAR), coupled to its good detection performance in a wide range of incidence angles and weather conditions, provide an ideal solution for obstacle avoidance, which is very attractive in low-level flying Unmanned Aircraft (UA).The first laser experiment directed towards a laser obstacle detection and avoidance system started in 1965 with a Nd:YAG laser [1]. This system demonstrated the feasibility of using lasers to detect obstacles such as wires. Semiconductor lasers, such as GaAs and GaAlAs have been experimented with since 1966 [2]. These lasers radiate in the wavelength region of 0.84 to 0.9μm. The experience gained with these experimental systems pointed out many features that are now being incorporated into present day research. Due to eye-safety and adverse weather (fog) propagation concerns, further development with Nd:YAG and the various semiconductor lasers has been substantially reduced, in favor of CO_2 lasers. One of the first heterodyne detection CO_2system was the LOWTAS, developed by UTRC. More recent developments include CLARA, the Anglo-French compact laser radar demonstrator program [3]; HIWA, a German system built and tested by Eltro and Dornier [4], and OASYS, developed in the U.S. by Northrop [5]. Current research efforts are concentrating on 1.54μm (frequency-shifted Nd:YAG and Er:glass) solid state lasers. One 1.54μm system has been developed for the Italian Military Forces by Marconi S.p.A., in cooperation with the Air Force Flight Test Centre. The equipment, here named LOAM (Laser Obstacle Avoidance Marconi), is a low-weight/volume navigation aid system for rotary-wing/UA platform specifically designed to detect potentially dangerous obstacle placed in or nearby the flight trajectory and to warn the crew in suitable time to implement effective avoiding maneuvers. The first airborne prototype of LOAM was assembled in 2005 and extensive laboratory and field tests were performed on the various sub-units, in order to refine the system design (both hardware and software components). Furthermore, the overall system was tested in flight on helicopter test-bed platforms [6], [8]. Current research is focusing on the development of a scaled LOAM variant for small to medium size UA applications.

II. Operational Requirements

As discussed in [6], the first and most important requirement for an airborne Obstacle Warning System (OWS) to be effective is reliable detection of all relevant obstacles in

R. Sabatini is Associate Professor in the School of Aerospace, Mechanical and Manufacturing Engineering, RMIT University, Melbourne, VIC 3000, Australia. Formerly, he was a Senior Officer and Experimental Flight Test Engineer in the Italian Air Force, Pratica di Mare AFB, 00040 Pomezia (RM), Italy (phone: +61 3 9925 8015; e-mail: roberto.sabatini@rmit.edu.au).

A. Gardi is a doctoral research student in Aerospace Engineering in the School of Aerospace, Mechanical and Manufacturing Engineering, RMIT University, Melbourne, VIC 3000, Australia.

M. A. Richardson is Full Professor and Head of the Sensors and Systems Engineering Department at Cranfield University, Defence Academy of the United Kingdom, Shrivenham, Swindon, UK.

a wide envelope of conditions defined primarily by the available laser range performance at various incidence angles and by the system Field-of-View (FOV). These parameters must be consistent with the aircraft dynamics envelope and produce a very high probability of detection and a very low false alarm rate. By all relevant obstacles, it is meant terrain masses, buildings, poles, towers, power cables and indeed any structure which may pose a hazard to low-level flying aircraft. The need for a high probability of detection is obvious since no real obstacle threat must go undetected. A low false alarm rate is required to prevent spurious warnings that would increase the pilot's workload unnecessarily and possibly cause the pilot to raise his altitude without real need, thus making him a better target in military operations requiring electromagnetic covertness. Another operational requirement is the minimum detection range. This will depend upon the aircraft speed, climb angle capability (different for helicopter, UA and airplane platforms), and pilot reaction time. As an example, for an airplane flying straight and level at 300m/sec and allowing a reasonable pilot reaction time and aircraft response time of between five to ten seconds, detection ranges of about two to three kilometers are adequate. For helicopter and UA applications, this range is generally reduced by an order of magnitude or more. The system should, ideally, perform all of its required functions in all weather, day and night. In practice however, laser radiation is not capable of all-weather operation and the best trade-off of system characteristics must be looked at.

III. LOAM System Description

LOAM system was originally developed for military rotorcraft platforms and, in the current study, we discuss some of the key aspects related to its potential design evolutions for integration in civil and military UA platforms. The general architecture of LOAM is depicted in Fig. 1.

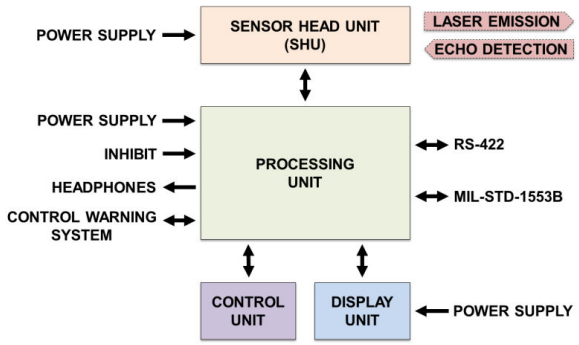

Fig. 1 General architecture of LOAM, adapted from [6]

LOAM is capable of detecting obstacles placed in or nearby the aircraft trajectory, classifying/prioritizing the detected obstacles, and providing obstacle warnings and information to the crew (both aural and visual). As depicted in Fig. 2, the laser beam scans periodically the area around the flight trajectory inside a Field of View (FOV) of 40° in azimuth and 30° in elevation with field of regard capability of ±20° both on azimuth and elevation, centered on the optical axis of the system).

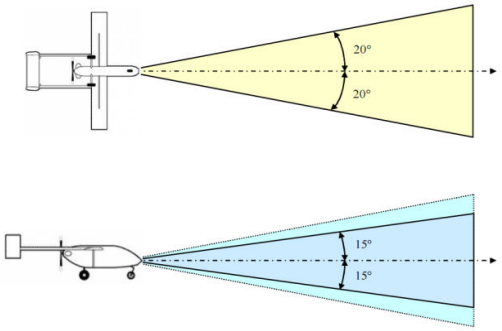

Fig. 2 LOAM Horizontal and Vertical FOV

LOAM also allows the operator to select the azimuth orientation of the FOV among three different directions, and in particular oriented either in the same direction of the platform heading (normal flight envelope), or 20° left/right with respect to the platform heading (to optimize coverage during turning maneuvers at high angular speed). This is represented in Fig. 3.

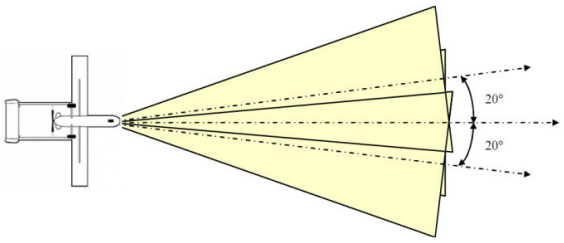

Fig. 3 LOAM FOV Orientation

During every scan (4 Hz repetition frequency), the laser beam changes its orientation producing an elliptical pattern across the FOV with the characteristics shown in Fig. 4.This scanning pattern is well suited to detect the most dangerous obstacles, like wires, due to the several and regularly spaced vertical lines that it produces. Additionally, it can be obtained by using very reliable scan mechanical devices with reduced weight.

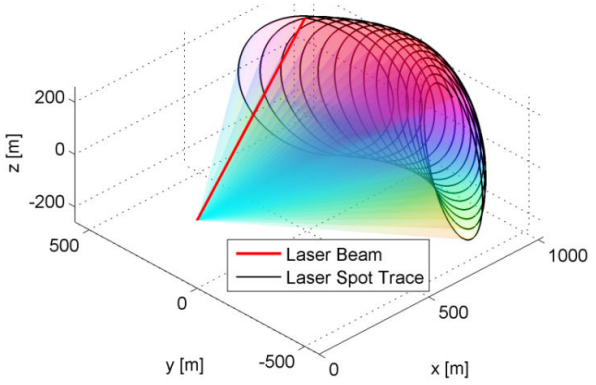

Fig. 4 LOAM Scan Pattern

Using dedicated signal processing algorithms optimized for low-level obstacle detection, the system holds an inherently high capacity to detected various types of obstacle independently from the platform motion during the frame acquisition period, providing the possibility of reconstructing the obstacle shape without using navigation data (stand-alone integration) in slow-moving platforms with a benign attitude envelope. Additionally, LOAM can be integrated with the aircraft navigation sensors if required, especially in platforms with high dynamics envelopes [8].LOAM performs echo detection through an analogue process comprising an optical-electrical conversion, a signal pre-amplification and a threshold comparison. The signal pre-amplification is achieved by an automatic controlled gain amplifier to increase the system sensitivity as the elapsed time from the laser emission increases in order to adjust the sensitivity on the basis of the expected return signal power in connection with the obstacle range. Furthermore, an adjustable threshold level is provided to take into account the background conditions. These features reduce the probability of false echo detection due to the atmospheric back-scatter near the laser beam output and optimize the system sensitivity in various operational weather conditions. LOAM performs echo analysis in order to determine the presence of possible obstacles and to determine their geometrical characteristics and position. For this purpose, LOAM operates through two sequential analysis processes: Local Analysis (LAN) and Global Analysis (GAN).The LAN process is performed on the single echoes in order to determine range, angular coordinates and characteristics of the obstacle portion generating them. The GAN process manages groups of echoes, detected during a scan period, with the related information provided by the LAN process, in order to perform the obstacle detection as a whole and determine the related shape and type. LOAM is capable to automatically classify obstacles according to the following classes [8]:

1) **Wire.** This class groups all thin obstacles like wires and cables (e.g., telephone/electrical cables and cableway);
2) **Tree.** This class groups vertical obstacles of reduced dimensions (e.g., trees, poles and pylons);
3) **Structure.** This class groups extended obstacles (e.g., bridges, buildings and hills).

Fig. 5 represents LOAM detection algorithm structure. Furthermore, LOAM performs automatic prioritization of the detected obstacles in function of the risk represented according to the relevant range, and provides the crew with timely warnings and information of the detected obstacles in order to allow the implementation of effective avoidance maneuvers. For this purpose, LOAM system is able to deliver both visual and audio warnings. LOAM information relative to the detected obstacles can be provided on a dedicated display (NVG compatible) whose screen represents the FOV of the system.

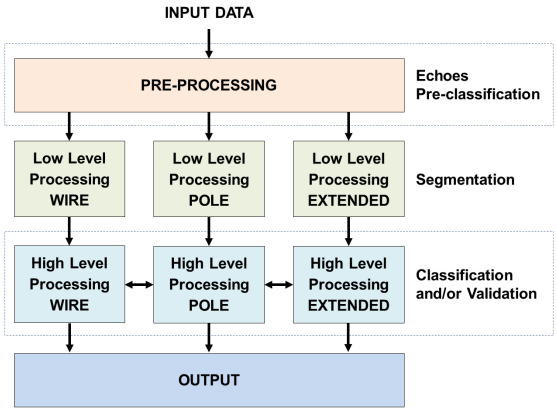

Fig. 5 Structure of LOAM detection algorithm

Both 3-D and 2-D are possible, together with an altimetric profile format. An example of a 3-D LOAM display format implemented for the already developed helicopter applications is shown in Fig. 6 [6]. The corresponding 2-D and altimetric display formats are shown in Figs. 7 and 8 respectively. The general architecture of LOAM system was described in [6]. LOAM main components are the Sensor Head Unit (SHU), the Control Panel (CP) and the Display Unit (DU). In the following paragraph a brief description of LOAM SHU is given, together with an outline of the main EPU functions.

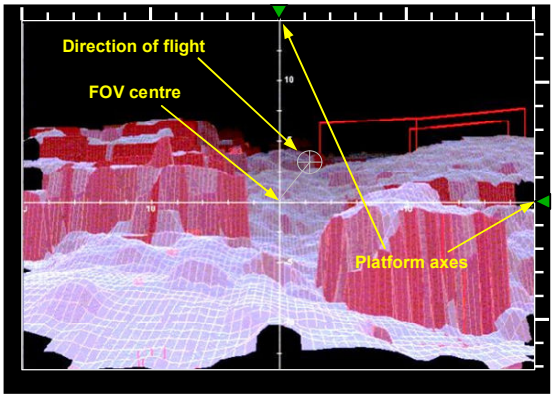

Fig. 6 LOAM 3-D Display Format

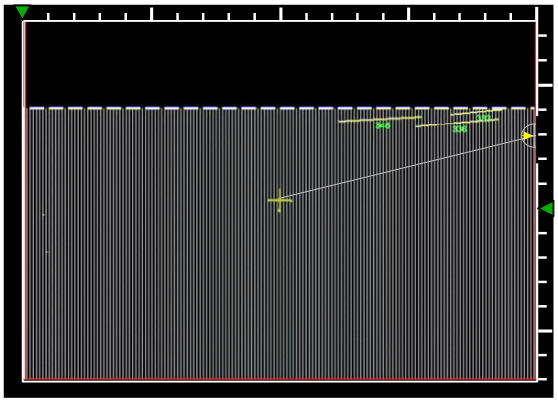

Fig. 7 LOAM 2-D Display Format

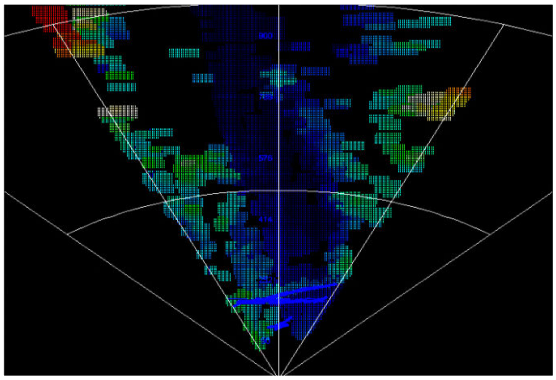

Fig. 8 LOAM Altimetric Display Format

The SHU performs the following main functions [8]:

1) generates a laser beam and scan the area around the flight trajectory;
2) detects return echoes;
3) analyzes detected echoes in order to compute range, coordinates and local geometrical characteristics (attributes) of the obstacles they come from;
4) communicates echo range, coordinates and attributes to LOAM Processing Unit, or to other on board systems, via a RS-422 high speed serial data link.

The SHU scans a laser beam in the area around the flight trajectory, performs echo detection through an analogue process comprising an optical-electrical conversion (by means of an avalanche photodiode - APD), a signal pre-amplification and a threshold comparison (adjustable threshold).The SHU performs echo analysis in order to compute range, coordinates (azimuth, elevation with respect to LOAM reference frame) and local geometrical characteristics (attributes) of the obstacles they come from. A detailed description of LOAMSHU architecture is presented in [6]. Some key electro-optical parameters relative to the laser sub-unit are listed in Table I.

TABLE I
LASER PARAMETERS

Parameter	Description	Value
Wavelength	Laser emission wavelength	1.55μm
Peak Power	Laser pulse power at the laser assembly output	10 kW
Pulse Duration	Laser pulse duration	3 to 5 ns
Frequency	Laser pulse repetition frequency	60 kHz

IV. CALCULATION OF AVOIDANCE TRAJECTORIES

Once the obstacle has been detected and processed as described, LOAM system triggers the generation of an avoidance trajectory, based on the own vehicle dynamics and the obstacle relative equation of motion. Due to the restricted system FOV, some information, acquired in the previous frame, may be lost successively. To keep obstacles information when they are outside the present frame, it is necessary to store the position of every object detected and then update the coordinates with respect to the platform body-fixed reference system. LOAM history function stores the data of the obstacles for a defined time interval and deletes them when they are outside the platform possible trajectories (outside its flight envelope).

Since the motion data supplied from navigation system are, like every measure, affected by an error, we evaluate how these errors affect the positions calculated for every obstacle. To do so, a Gaussian error is added to every data and a statistic of the position error is calculated for obstacles near and far from the aircraft. When the impact warning processing establishes that the trajectory currently flown by the aircraft has a collision risk, the algorithm searches the corrections necessary to avoid the obstacles, and provides the pilot an indication about the alternative (optimal) direction to fly. The optimal trajectory is the one having the smaller possible correction (necessary to avoid the obstacles) and which is compatible with a safe flight path.

The original avoidance trajectories generation algorithm for helicopter platforms was introduced in [6]. In this paper we present the key aspects of the avoidance trajectory generation algorithm for UA applications. The approximated dynamic model of LOAM equipped UA platform for avoidance trajectory generation purposes is derived by introducing the following assumption:

- The UA is modeled as a point-mass rigid body with three linear degrees of freedom (3DOF);
- The inertial reference system is centered on the initial position of the UA point-mass, with the X axis pointing eastward, the Y axis northward and the Z axis normal to the ground;
- The UA is subject to a constant gravitational acceleration parallel and opposite to the Z axis, and for the purpose of our estimation we assume $g = 9.81\ m/s^2$;
- The mass of the vehicle is considered constant along the avoidance trajectory;
- During the avoidance maneuver, the load factor is set close to the certified flight envelope limits of the UA. In our case these correspond to $N = N_{MAX} = 2.5$ for the pull-up maneuvers and $N = N_{MIN} = -1$ for the diving maneuvers;
- The airspeed of the UA is expressed as True Air Speed (TAS). The wind is not explicitly expressed, although implicitly considered in the vehicle-obstacle relative motion. In our case, the assumed initial TAS is $v = 25\ m/s$.

The resulting system of differential equations for 3DOF vehicle dynamics is:

$$\begin{cases} \dot{v} = \frac{F_X}{m} - g \cdot sin\gamma \\ \dot{\gamma} = \frac{g}{v}(N \cdot cos\mu - cos\gamma) \\ \dot{\chi} = \frac{g}{v} \cdot \frac{N \cdot sin\mu}{cos\gamma} \\ \dot{x} = v \cdot cos\gamma \cdot sin\chi \\ \dot{y} = v \cdot cos\gamma \cdot cos\chi \\ \dot{z} = v \cdot sin\gamma \end{cases} \quad (1)$$

where:

- F_X= sum of aerodynamic/propulsive forces along X axis;
- γ = flight path angle;
- χ = track angle;

- μ = bank angle.

We then assume that during the entire approach to the obstacle, the vehicle control system can provide a linear variation of μ, up to the assumed maximum bank angle. This can be expressed as:

$$\begin{cases} \mu = \mu_0 + \dot{\mu}_{MAX} \cdot t & (\mu \leq \mu_{MAX}) \\ \dot{\mu} = 0 & (\mu = \mu_{MAX}) \end{cases} \quad (2)$$

The maximum roll rate was set at $\dot{\mu}_{MAX} = 20\,°/s$. The maximum bank angle was simply calculated as:

$$\mu_{MAX} = \operatorname{acos}\left(1/N_{MAX}\right) \quad (3)$$

The algorithms for estimation of the obstacle absolute motion based on differential geometry approach were introduced in [12]. In order to provide the fast and reliable performance required for our safety-critical task, the avoidance trajectory generation is based on simplified geometric shapes. In particular, given the different values of uncertainty associated with the three cardinal directions, an ellipsoidal avoidance volume is implemented in the algorithm. The standard deviation of LOAM detection and tracking error for each axis is given by:

$$\sigma_{(X,Y,Z)} = \sqrt{\sigma^2_{range_{(x,y,z)}} + \sigma^2_{bearing_{(x,y,z)}} + \sigma^2_{other_{(x,y,z)}}} \quad (4)$$

In order to assure adequate safety levels, a separation buffer is introduced, which inflates the ellipsoidal avoidance volume associated with the obstacle. In particular, to provide a confidence level of 95%, the uncertainty associated with the position of an obstacle is calculated as twice the standard deviation (i.e. the two-sigma) of the total obstacle detection and tracking errors. When the distance between two detected obstacles is comparable with the calculated uncertainty values, or with the UA dimensions, the algorithm combines the two obstacles in a single avoidance volume. The subsequent step involves the selection of the optimal trajectory from the generated set of safe trajectories, which is then fed to the aircraft guidance subsystems. The implemented decision logic is based on minimization of the following cost function:

$$J = w_t \cdot t_{SAFE} + w_f \int [SFC \cdot T(t)]dt - w_d \int D(t)dt \quad (5)$$

where:

- t_{SAFE} is the time at the minimum distance point to the obstacle, hence it corresponds to the attainment of a safe condition;
- $SFC\ [\frac{kg}{N} \cdot s]$ is the specific fuel consumption;
- $T(t)$ is the thrust profile;
- $D(t) = \sqrt{\left[\frac{(x(t)-x_{obs})^2}{d^2_{MINx}} + \frac{(y(t)-y_{obs})^2}{d^2_{MINy}} + \frac{(z(t)-z_{obs})^2}{d^2_{MINz}}\right]}$ is the distance from the ellipsoidal avoidance volume of the obstacle;
- w_t, w_f, w_d are the weightings attributed to time, fuel and integral distance respectively.

In time-critical avoidance applications (i.e., closing-up obstacles with high relative velocities and/or accelerations) appropriate higher weightings are used for the time and distance cost elements.

V. Simulation and Results

Simulation activities were performed to validate the avoidance trajectory generation algorithm and to assess its performance. A realistic three-dimensional scenario for obstacle avoidance is depicted in Fig. 9. The UA equipped with LOAM is flying at an altitude z = 100 m Above Ground Level (AGL) and approaching a power transmission line consisting of a number of wires of 10mm in diameter. The altitude of the lowest wire is 95m AGL and the altitude of the highest wire is 115m AGL; the wires are separated by about 6.5m vertically and 5m laterally. The transmission line lies approximately 70m in front of the UA. The original horizontal flight trajectory would lead to a collision with the obstacle.

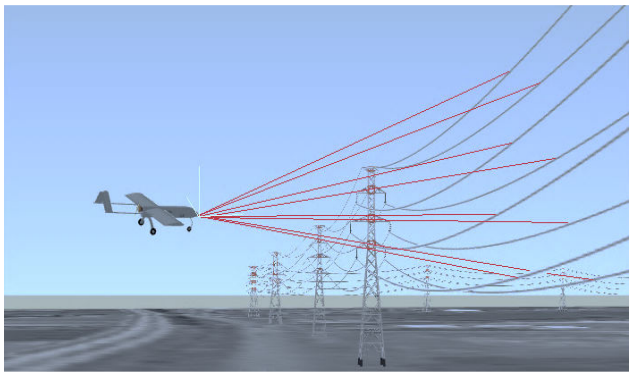

Fig. 9 Representation of LOAM system wire detection from a mini-UA

After a successful detection of all the wires, the algorithm calculates the distances among each of them. As previously described the algorithm then recognizes that the calculated distances are all comparable with the UA wingspan (3 meters) and therefore combines all the wires in a single obstacle. The centre C position and the semi-major axis a, b, c of the resulting ellipsoidal avoidance volume are then calculated. In particular C = {70m, 0m, 105m}; a = 15m; b = 100m; c = 25m. A representative set of avoidance trajectories generated following these assumptions, is depicted in Fig. 10.

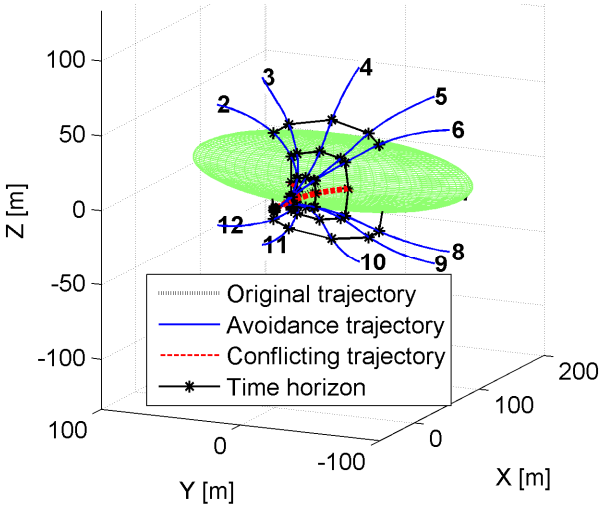

Fig. 10 Valid and conflicting trajectories in the UA reference system

Fig. 11 shows the separation envelopes between the UA and the boundary surface of the ellipsoidal avoidance volume, calculated for each point of the UA conflicting and avoidance trajectories.

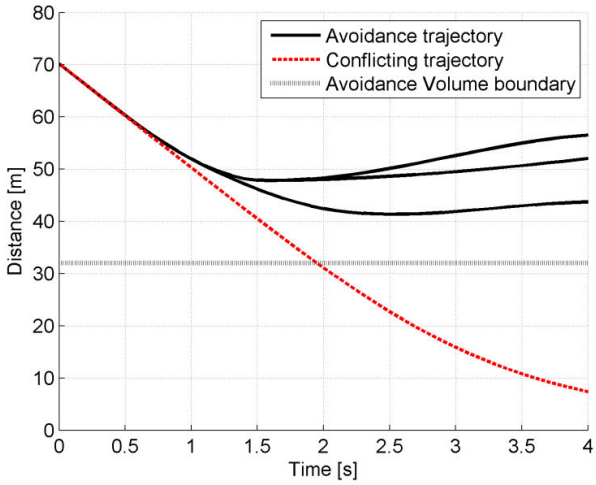

Fig. 11 Absolute distance of the generated trajectories from the ellipsoidal avoidance volume boundary

VI. LOAM Performance Evaluation

The mathematical derivation of the various phenomena affecting LOAM laser beam in all the atmospheric conditions were derived and discussed for different applications in [7]-[11]. As detailed in [6], ground trials of LOAM system were performed in order to verify the system detection performance in various weather conditions, and to test the validity of the mathematical models used for performance calculations. This was particularly important for preparing LOAM system flight test activity. It is in fact necessary to define a criteria for determining the system detection range performances in the worst environmental conditions, and with the worst obstacle scenarios (i.e., small wires with low reflectivity), even without performing real tests in these conditions (i.e., using experimental data collected in fear weather and with average obstacles). Mathematical modeling and ground testing of LOAM system detection performance are therefore required in order to derive the involved parameters and estimate the target LOAM system detection performances to be demonstrated in the flight testing. The modeling activities are detailed in [6]. Analogously, the following definitions are adopted for a wire type obstacle in line with LOAM system operational requirements:

- Diameter: 5 mm $\leq D_W \leq$ 70 mm
- Shape: Twisted or round
- Reflection: Purely diffuse (Lambertian)
- Reflectivity: $\geq$ 20% (θ = 0)

The reference environmental parameters are the following:

- Visibility: V $\geq$ 800 m
- Humidity: RH $\leq$ 100%
- Temperature: T $\leq$ 50 °C
- Rain: Light/Medium/Heavy
- Background: P_B = 50 W/m^{2}srμm

Ground trials of LOAM system were performed in order to verify the system detection performance in various weather conditions, and to test the validity of the mathematical models used for performance calculations. This was particularly important for preparing LOAM flight test activity. It was in fact necessary to define a criteria for determining the system detection range performances in the worst environmental conditions, and with the worst obstacle scenarios (i.e., small wires with low reflectivity), even without performing real tests in these conditions (i.e., using experimental data collected in fear weather and with average obstacles). Mathematical modeling and ground testing of LOAM detection performance were therefore required in order to give proper weights to the parameters playing a role in realistic operational scenarios, and to determine the target LOAM detection performances to be demonstrated in flight. Fig. 12 illustrates the process involved.

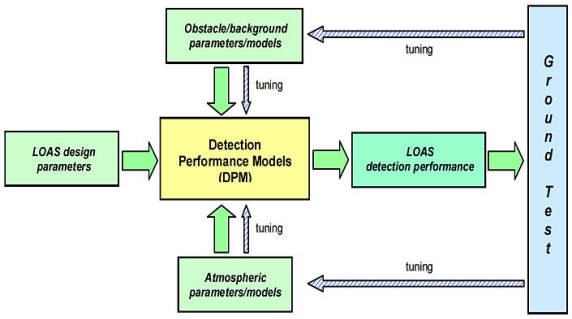

Fig. 12 Detection performance models and ground test

As the ground test activities permitted to validate the models developed, it was then possible to identify reference sets of obstacle, background and atmospheric parameters giving the absolute minimum performance of LOAM system. This is illustrated in Fig. 13. Obviously, the successive flight

test activities were performed only in a small portion of LOAM operational envelopes, but the results obtained could be extended to the entire envelopes by using the validated mathematical models.

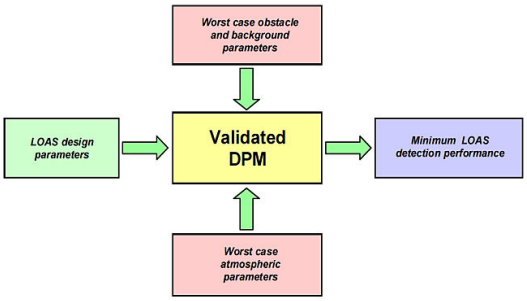

Fig. 13 Minimum detection performance calculation

For initial design calculations, the wire obstacle detection capability of LOAMis modelled by the following simplified Signal to Noise Ratio (SNR) equation:

$$SNR = \frac{4E_p A_r L_T L_r e^{-2\gamma R} d_W \rho}{\pi P_D R^2 (\alpha R + D) NEP} \quad (6)$$

where:

E_P = output laser pulse energy
A_r = receiver aperture
L_T = transmission losses (including beam shaping)
L_r = reception losses (including optical filter)
γ = atmospheric extinction coefficient
d_W = wire diameter
ρ = wire reflectivity
P_D = pulse duration
R = obstacle range
α = beam divergence (l /e2)
D = initial beam diameter
NEP = noise equivalent power

The extinction coefficient (γ) is calculated as described in [8], including the propagation in rainy conditions. This approach (ESLM model) is particularly useful because it provides a means of relating the atmospheric transmission of the i^{th} window to the atmospheric visibility, relative humidity and rainfall-rate (i.e., readily measurable parameters). The first assumption made [8] is that variations in the transmission are caused by changes in the water content of the air. Specifically, changes in the concentration of H_2O cause changes in the absorption, and changes in the size and number of water droplets with humidity cause changes in the scattered component. This is a valid assumption since the other atmospheric constituents have a reasonably constant effect on the transmittance of a given atmospheric window.

It is customary to express the number of H_2O molecules encountered by the beam of light in terms of the number of precipitable millimeters of water in the path. Specifically, the depth of the layer of water that would be formed if all the water molecules along the propagation path were condensed in a container having the same cross-sectional area as the beam is the amount of precipitable water. A cubic meter of air having an absolute humidity of ρ grams per m^3 would yield condensed water that cover a l m^2 area and have a depth of:

$$w' = 10^{-3}\rho \quad (7)$$

where w' is the precipitable water having units of mm per meter of path length. For a path length of z meters eq. 12 becomes:

$$w = 10^{-3}\rho \cdot z \quad (8)$$

where w is now the total precipitable water in millimeters. The value of ρ, the density of water vapor, can be obtained using the following equation [6], which is convenient for computer code implementation:

$$\rho = 1322.8 \cdot \frac{RH}{T} e^{\left[\frac{25.22(T-273.16)}{T} - 5.31 \ln\left(\frac{T}{273.16}\right)\right]} \quad (9)$$

where RH is the relative humidity (as a fraction), and T is the absolute temperature (°K). Two empirical expressions, developed by Langer [9], can be used to calculate the absorptive transmittance τ_{ai} for the i^{th} window for any given value of the precipitable water content. These expressions are:

$$\tau_{ai} = e^{-A_i\sqrt{w}}, \text{ for } w < w_i \quad (10)$$

$$\tau_{ai} = k_i \left(\frac{w_i}{w}\right)^{\beta_i}, \text{ for } w > w_i \quad (11)$$

where A_i, k_i, β_i and w_i are constants whose values for each atmospheric window are listed in [8]. For LOAM laser wavelength (λ = 1550nm - 4th atmospheric window), A_i = 0.211, k_i= 0.802, β_i = 0.111 and w_i = 1.1. In summary, (10) and (11), together with (8) and (9), provide information that can be used to obtain an estimate of the absorptive transmittance (τ_{ai}) of laser beams having wavelengths that fall within the various atmospheric windows. The results apply to horizontal paths in the atmosphere near sea-level and for varying relative humidity. To obtain the total atmospheric transmittance we must multiply τ_{ai} by τ_{si}(i.e., the transmittance due to scattering only).

Based on rigorous mathematical approaches, the scattering properties of the atmosphere due to the aerosol particles are difficult to quantify, and it is difficult to obtain an analytic expression for the scattering coefficient that will yield accurate values over a wide variety of conditions. However, an empirical relationship that is often used to model the scattering coefficient has the form:

$$\beta(\lambda) = C_1\lambda^{-\delta} + C_2\lambda^{-4} \quad (12)$$

where C_1, C_2, and δ are constants determined by the aerosol concentration and size distribution, and λ is the wavelength of the radiation. The second term accounts for *Rayleigh* scattering. Since for all wavelengths longer than about 0.3 μm the second term is considerably less than the first, it may be neglected. It has been found that $\delta \approx 1.3 \pm 0.3$ produces reasonable results when applied to aerosols with a range of particle sizes. An attempt has also been made to relate $\delta$and C_1 to the meteorological range. The apparent contrast C_z, of a source when viewed at λ = 0.55μm from a distance z is by definition:

$$C_z = \frac{R_{sz} - R_{bz}}{R_{bz}} \tag{13}$$

where R_{sz} and R_{bz} are the apparent radiances of the source and its background as seen from a distance z. For $\lambda = 0.55\,\mu\text{m}$, the distance at which the ratio:

$$V = \frac{C_z}{C_0} = \frac{\frac{R_{sz} - R_{bz}}{R_{bz}}}{\frac{R_{s0} - R_{b0}}{R_{b0}}} = 0.02 \tag{14}$$

is defined as the meteorological range V (or visual range). It must be observed that this quantity is different from the standard observer visibility (V_{obs}). Observer visibility is the greatest distance at which it is just possible to see and identify a target with the unaided eye. In daytime, the object used for V_{obs} measurements is dark against the horizon sky (e.g., high contrast target), whereas during night time the target is a moderately intense light source. The International Visibility Code (IVC) is given in Table II.

TABLE II
INTERNATIONAL VISIBILITY CODE

Designation	Visibility
Dense Fog	0 – 50 m
Thick Fog	50 – 200 m
Moderate Fog	200 – 500 m
Light Fog	500 – 1 km
Thin Fog	1 – 2 km
Haze	2 – 4 km
Light Haze	4 – 10 km
Clear	10 – 20 km
Very Clear	20 – 50 km
Exceptionally Clear	> 50 km

It is evident that, although the range of values for each category is appropriate for general purposes, it is too broad for scientific applications. Visibility is a subjective measurement estimated by a trained observer and as such can have large variability associated with the reported value. Variations are created by observers having different threshold contrasts looking at non-ideal targets. Obviously, visibility depends on the aerosol distribution and it is very sensitive to the local meteorological conditions. It is also dependent upon the view angle with respect to the sun. As the sun angle approaches the view angle, forward scattering into the line-of-sight increases and the visibility decreases. Therefore, reports from local weather stations may or may not represent the actual conditions at which the experiment is taking place. Since meteorological range is defined quantitatively using the apparent contrast of a source (or the apparent radiances of the source and its background) as seen from a certain distance, it eliminates the subjective nature of the observer and the distinction between day and night. Unfortunately, carelessness has often resulted in using the term Visibility when Meteorological Range is meant. To insure that there is no confusion, Observer Visibility (V_{obs}) will be used in this thesis to indicate that it is an estimate. If only $V_{obs}$is available, the meteorological range (V) can be estimated [11] from:

$$V \approx (1.3 \pm 0.3) \cdot V_{obs} \tag{15}$$

If we assume that the source radiance is much greater than the background radiance (i.e., $R_s >> R_b$) and that the background radiance is constant (i.e., $R_{bo} = R_{bz}$), then the transmittance at λ = 0.55μm (where absorption is negligible) is given by:

$$\frac{R_{sv}}{R_{s0}} = e^{-\beta V} = 0.02 \tag{16}$$

Hence, we have:

$$\ln\left(\frac{R_{sv}}{R_{s0}}\right) = -\beta V = -3.91 \tag{17}$$

and also:

$$\beta = \frac{3.91}{V} = C_1 \lambda^{-\delta} \tag{18}$$

It follows from (29) that the constant C_1 is given by:

$$C_1 = \frac{3.91}{V} \cdot 0.55^{\delta} \tag{19}$$

With this result the transmittance at the centre of the i^{th} window is:

$$\tau_{si} = e^{-\frac{3.91}{V}\left(\frac{\lambda_i}{0.55}\right)^{-\delta} \cdot z} \tag{20}$$

where λ_i must be expressed in microns. If, because of haze, the meteorological range is less than 6km, the exponent δ is related to the meteorological range by the following empirical formula:

$$\delta = 0.585\sqrt[3]{V} \tag{21}$$

where V is in kilometers. When $V \geq$ 6km, the exponent δ can be calculated by:

$$\delta = 0.0057 \cdot V + 1.025 \quad (22)$$

For exceptionally good visibility δ = 1.6, and for average visibility $\delta \approx$ 1.3. For LOAM, it is also very important to model propagation through haze and precipitation. Haze refers to the small particles suspended in the air. These particles consist of microscopic salt crystals, very fine dust, and combustion products. Their radii are less than 0.5μm. During periods of high humidity, water molecules condense onto these particles, which then increase in size. It is essential that these condensation nuclei be available before condensation can take place. Since salt is quite hygroscopic, it is by far the most important condensation nucleus. Fog occurs when the condensation nuclei grow into water droplets or ice crystals with radii exceeding 0.5μm. Clouds are formed in the same way; the only distinction between fog and clouds is that one touches the ground whereas the other does not. By convention fog limits the visibility to less than 1km, whereas in a mist the visibility is greater than 1km. We know that in the early stages of droplet growth the Mie attenuation factor *K* depends strongly on the wavelength. When the drop has reached a radius a ≈ 10 λ the value of *K* approaches 2, and the scattering is now independent of wavelength, i.e., it is nonselective. Since most of the fog droplets have radii ranging from 5 to 15μm they are comparable in size to the wavelength of infrared radiation. Consequently the value of the scattering cross section is near its maximum.It follows that the transmission of fogs in either the visible or *IR* spectral region is poor for any reasonable path length.This of course also applies to clouds. Since haze particles are usually less than 0.5μm, we note that for laser beams in the *IR* spectral region $a/\lambda << 1$ and, therefore, scattering is not the dominating attenuation mechanism. The scattering coefficient with rain, however, depends strongly on the size of the drop and it can be approximated by:

$$\beta_{rain} = 1.25 \cdot 10^{-6} \frac{\Delta x / \Delta t}{a^3} \quad (28)$$

where $\Delta x/\Delta t$ is the rainfall rate in centimeters of depth per second and *a* is the radius of the drops in centimeters. Rainfall rates for four different rain conditions and the corresponding transmittance (due to scattering only) of a 1.8-km path are shown in Table III [11].

TABLE III
TRANSMITTANCE OF A 1.8 KM PATH THROUGH RAIN

Rainfall (cm/h)	Transmittance (1.8 km path)
0.25	0.88
1.25	0.74
2.5	0.65
10.0	0.38

These data are useful for order of magnitude estimates. In order to obtain accurate estimates, the concentrations of the different types of rain drops (radius) and the associated rainfall rates should be known. In this case, the scattering coefficient can be calculated as the sum of the partial coefficients associated to the various rain drops.A simpler approach, used in LOWTRAN, gives good approximations of the results obtained for most concentrations of different rain particles. Particularly, the scattering coefficient with rain has been empirically related only to the rainfall rate $\Delta x/\Delta t$ (expressed in mm/hour), as follows [10]:

$$\beta_{rain} \approx 0.365 \cdot \left(\frac{\Delta x}{\Delta t} \right)^{0.63} \quad (29)$$

Table IV provides representative rainfall rates which can be used when no direct measurements are available, to obtain order of magnitude estimations of β_{rain}.

TABLE IV
REPRESENTATIVE RAINFALL RATES

Rain Intensity	Rainfall (mm/hour)
Mist	0.025
Drizzle	0.25
Light	1.0
Moderate	4.0
Heavy	16
Thundershower	40
Cloud-burst	100

In the presence of rain, in addition to the scattering losses, there are, of course, losses by absorption along the path, and these must be included in the calculation of the total atmospheric transmittance with rain.

In order to estimate the SNR from experimental LOAM detector current measurements (i_{SIG}), obtained with certain obstacle ranges (R) and incidence angles (θ), SNR was expressed as follows:

$$SNR = 20 \log \left(\frac{i_{SIG}(R,\theta)}{i_{NOISE}} \right) \quad (30)$$

The noise current terms in (2) was modeled as:

$$i_{NOISE} = \sqrt{i_{TH}^{\ 2} + i_{BK}^{\ 2} + i_{DK}^{\ 2} + i_{RA}^{\ 2}} \quad (31)$$

where:

i_{TH} = thermal noise current
i_{BK} = background noise current
i_{DK} = dark noise current
i_{RA} = receiver amplifier noise

According to LOAM design characteristics, we have:

$$i_{BK} = \sqrt{2qP_S P_h M_A (2 + kM_A) B} \quad (32)$$

$$i_{TH} = \sqrt{4K_B \frac{T_k Bk}{R_L}} \quad (33)$$

$$i_{DK} = 0.5 \cdot 10^{-12} \quad (34)$$

$$i_{RA} = 1.5 \cdot 10^{-12} \quad (35)$$

where:

P_S = received solar power
P_h = amplifier gain
M_A = avalanche multiplier
k = noise factor of the avalanche photodiode
B = electronic bandwidth
K_B = Boltzmann constant (1.39×10-23 J/°K)
T_k = absolute temperature (°K)
R_L = amplifier load resistance

For calculation purposes, the $i_{SIG}(R,\theta)$ term was modeled as:

$$i_{SIG} = \sqrt{\frac{P_T d_W \rho D_a^3 \eta e^{-2\gamma R}}{4R^3 \lambda} \cdot \frac{P_h}{K_a} \cdot \frac{1}{R_L}} \quad (36)$$

where:

P_T = transmitted power
P_h = amplifier gain
D_a = aperture diameter
K_a = aperture illumination constant = $\sin(\theta)^{5.4}$

The estimated range performances of LOAM for cable obstacles having diameters (D_W) of 5mm and 10mm, in various visibility conditions and with all other parameters set to the worst case are shown in Fig. 12.

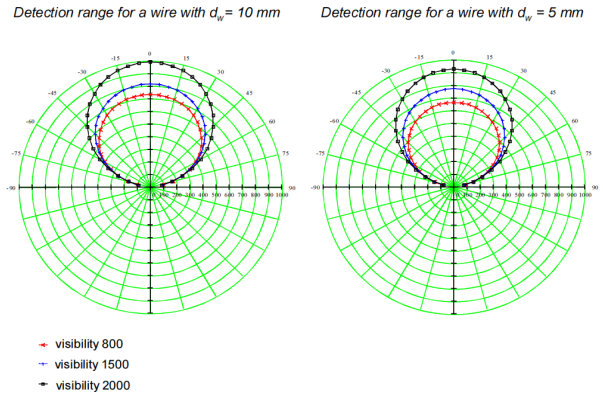

Fig. 14 LOAM estimated detection range performance for wires

The false alarm probability is modeled as:

$$P_{fa} = \frac{1}{B \cdot T_{fa} \cdot \eta} \quad (37)$$

where:

B = receiver bandwidth
T_{fa} = mean time between false alarms
η = maximum useful/nonambiguous range

The mean time between false alarms corresponds to electrical false alarms at the receiver level. The probability to have several false alarms on a straight line pattern is much lower. Statistically, these phenomena are described by the False Alarm Rate (FAR) and detection probability (P_d). If the noise and signal distributions are known, the Signal-to-Noise Ratio (SNR) can be estimated and the corresponding P_d and FAR can be determined. The average FAR of LOAM system can be written as:

$$\overline{FAR} = \frac{1}{2\tau\sqrt{3}} \exp\left(-\frac{I_t^2}{2I_n^2}\right) \quad (38)$$

where:

τ = Electrical pulse length
I_t = Threshold current
I_n = Average noise current

LOAM P_d is determined using pure Gaussian statistics:

$$P_d = \frac{1}{\sqrt{\pi}} \int_{\frac{I_t - I_n}{\sqrt{2}I_n}}^{\infty} \exp\left(-\frac{i_n^2}{2I_n^2}\right) d\left(\frac{i_n}{\sqrt{2}I_n}\right) \quad (39)$$

I_n = average signal current
i_n = instantaneous noise current

The false alarm probability (P_{fa}) is given by:

$$P_{fa} = \tau \cdot \overline{FAR} \quad (40)$$

and the cumulative detection probability (P_D) is given by:

$$P_D = 1 - \sum_{i=0}^{m} C_M^i P_d^i (1 - P_d)^{M-i} \quad (41)$$

where:

M = number of possible detections
m = minimum number of detections required

The scenario in which ground tests were performed is shown in Fig. 15.

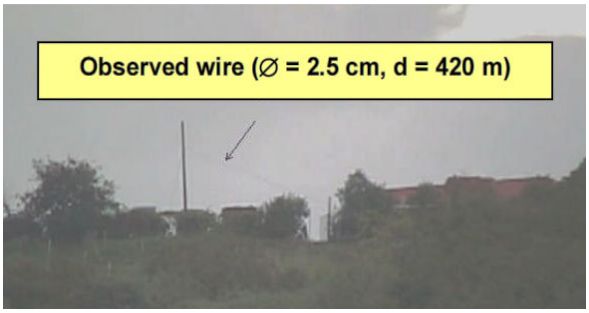

Fig. 15 LOAM ground tests scenario

A comparison between the SNR predicted (SNR_P) with γ calculated using the ESLM model ($0.19km^{-1} \leq \gamma \leq 0.22km^{-1}$ for clear weather and $1.23km^{-1} \leq \gamma \leq 2.94km^{-1}$ for rainy conditions), assuming a background power of 10 Watt/m^2/sr/μm and ρ = 0.5, and estimated from experimental data (SNR_E), is shown in Table V.

TABLE V
LOAM PREDICTED AND MEASURED SNR

	Clear Weather			Rain		
	V=10km	V=12.5km	V=15km	Light	Medium	Heavy
SNR_P	4.90×10^4	4.95×10^4	5.02×10^4	3.14×10^4	1.83×10^4	1.45×10^4
SNR_E	3.35×10^4	3.80×10^4	4.27×10^4	2.87×10^4	2.47×10^4	2.13×10^4

VII. FLIGHT TEST ACTIVITIES

Figs. 16 and 17 show LOAM prototype used for the helicopter flight trials. Particularly, LOAM sub-units are shown in Fig. 16 and the pilot interface units are shown in Fig. 17.

Fig. 16 Sub-units of LOAM prototype

Fig. 17 Prototype pilot interface units and SHU assembly

Two different test-bed platforms were used for the trials: the NH-300 and AB-212 helicopters. Fig. 18 shows LOAMSHU mounted on the AB-212.

Fig. 18 LOAM installed on AB-212

As shown in Fig. 19, the Cockpit Display Unit (CDU) used for the trials was installed at the centre of the AB-212 glare shield in order to be accessible to both pilot and co-pilot.For the AB-212 test campaign, LOAM Main Control Unit (MCU) was installed in the centre of the middle-consolein a position accessible to both pilot and co-pilot, as shown in Fig. 20. During the test flights, a Flight Test Engineer also operated a computer, linked to LOAM system and displaying in real-time a 3-dimensional image reconstructed using LOAM data. All images were also recorded for post-flight data analysis. The results of this test campaign were satisfactory. LOAM range performances were in accordance with the model predictions and LOAM detection/classification data processing algorithms were validated. Furthermore, it was verified that LOAM History Function was correctly implemented.

Fig. 19 Display unit installed on AB-212 glareshield

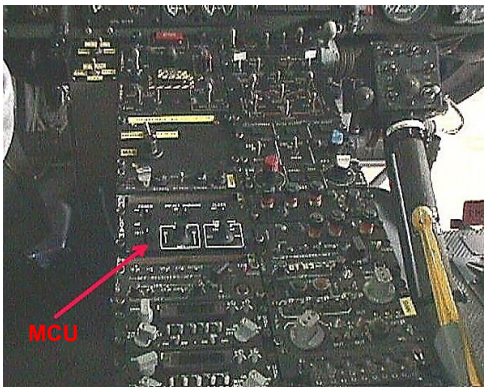

Fig. 20 LOAM Main Control Unit on AB-212

More detailed results of LOAM ground and flight test activities performed on various dedicated test-bed platforms are presented in [6] and [8].

VIII. CONCLUSIONS AND FUTURE WORK

The challenges and opportunities associated with the introduction of laser-based obstacle warning and avoidance systems in Unmanned Aircraft (UA) are discussed in this paper. Specifically, we have addressed the potential hardware and software design tailoring of an existing system: The Laser

Obstacle Avoidance Marconi (LOAM) developed and tested by SELEX-ES and the Italian Air Force Experimental Flight Test Centre. In particular, some preliminary mathematical models for UA flight dynamics and avoidance trajectory generation have been described. The original system design, including the requirements, the architecture, the components, the algorithms is summarized together with the ground testing and flight testing activities performed. Future ground and flight tests will be performed in order to assess the performance of LOAM system integrated on the various other flying platforms in day/night with various weather/environmental conditions and to optimize the ground operator Human Machine Interface (HMI) design. For future UA test flights, a dedicated control unit is also being designed to be integrated in the ground-based pilot station. Its characteristics are similar to the MCU developed and presented in [6]. However, as this MCU has to be operated by the ground UA pilot, in this case LOAM operating modes are activated using two different communication data links for Line-of-Sight (LOS) and Beyond LOS operations. Additionally, LOAM display functions will be fully integrated in the UA remote control position and the required LOAM display formats displayed to the UA pilot in real-time. The potential interfaces between LOAM and other on-board/ground systems are also being investigated. The system was previously implemented in a stand-alone setup [8]. It is expected that for the high-dynamics UA applications, an extensive integration with the developed Sense-and-Avoid (SAA) system, described in [12], and with the low-cost multi-sensor UA navigation and guidance system including Vision Based Navigation (VBN) described in [13] and [14] will be fundamental. In order to attain unrestricted access to airspace, the UA will have to incorporate the SAA capabilities in a comprehensive avionics architecture that should also include the emerging Communication, Navigation, Surveillance, Air Traffic Management (CNS/ATM) systems. Current avionics and CNS/ATM research is therefore addressing the possible direct integration of LOAM and other avoidance systems with manned aircraft and UA Flight Controls/Autopilots and Flight Management Systems [15], [16], and with the next generation of ground-based Air Traffic Management (ATM) systems being conceived for 4-Dimensional Trajectory Planning, Negotiation and Validation (4-PNV) in line with the requirements set by the SESAR (Single European Sky ATM Research) and NextGen (Next Generation Air Transportation System) research initiatives in Europe and in the United States [17], [18].

ACKNOWLEDGMENT

The originaldevelopment and testing activity was funded by the Italian Ministry of Defence (MoD) under R&D contract No. 2097-22-12-2000. The authors wish to thank the personnel of SELEX-ES, LOT-ORIEL, the Italian Air Force Experimental Flight test Centre, and the Italian MoD Laser Test Range (PILASTER) for helping in the preparation and execution of the ground and flight test activities.

REFERENCES

[1] C. B. Kellington, "An Optical Radar System for Obstacle Avoidance and Terrain Following", *AGARDCP-148,*NATO Science and Technology Organization Ed., 1965.

[2] B. Goldstein and G. Dalrymple, "GaAs Injection Laser Radar",in *Proc. of the IEEE,*Vol. 55 No. 2,1967.

[3] G. Hogg, K. Harrison, and S. Minisclou, "The Anglo-French Compact Laser Radar Demonstrator Programme", *AGARDCP-563*, NATO Science and Technology Organization Ed., 1995.

[4] W. Büchtemann, and M. Eibert, "Laser Based Obstacle Warning Sensors for Helicopters", *AGARD CP-563*, NATO Science and Technology Organization Ed., 1995.

[5] S.L. Holder, and R.G. Branigan, "Development and Flight Testing of an Obstacle Avaoidance System for the U.S. Army Helicopters", *AGARDCP-563*, NATO Science and Technology Organization Ed., 1995.

[6] R. Sabatini, M.A. Richardsom andE. Roviaro, "Development and Flight Test of an Avionics LIDAR for Helicopter and UAV Low-Level Flight", Journal of Aeronautics &Aerospace Engineering, Vol.2, No.3, 2013.

[7] R. Sabatini, F. Guercio and S. Vignola, "Tactical Laser Systems Performance Analysis and Mission Management",*RTO-MP-046 - Advanced Mission Management and System Integration Technologies for Improved Tactical Operations*, NATO Science and Technology Organization Ed.,2000.

[8] R. Sabatini, and M.A. Richardson, "Airborne Laser Systems Testing and Analysis", *RTO-AG-160*, AGARDograph Series, Vol. 26, NATO Research and Technology Organization (RTO) – Systems Concepts and Integration Panel (SCI), 2010.

[9] R. Sabatini, M.A. Richardson, H. Jia, and D. Zammit-Mangion, "Airborne Laser Systems for Atmospheric Sounding in the Near Infrared", in *Proc. of the SPIE Photonics Europe 2012 Conference*, Brussels, Belgium, 2012.

[10] R. Sabatini and M.A. Richardson, "New Techniques for Laser Beam Atmospheric Extinction Measurements from Manned and Unmanned Aerospace Vehicles", Central European Journal of Engineering, Vol. 3, Iss.1, pp. 11-35, 2012.

[11] R. Sabatini and M.A. Richardson, "Novel Atmospheric Extinction Measurement Techniques for Aerospace Laser System Applications", Infrared Physics & Technology, Vol. 56, pp. 30-50, 2013.

[12] L. Rodriguez Salazar, R. Sabatini, S. Ramasamy and A. Gardi, "A Novel System for Non-Cooperative UAV Sense-And-Avoid", in *Proc. of the European Navigation Conference 2013 (ENC 2013)*, Vienna, Austria, 2013.

[13] R. Sabatini, S. Ramasamy, A. Gardi and L. Rodriguez Salazar, "Low-cost Sensors Data Fusion for Small Size Unmanned Aerial Vehicles Navigation and Guidance", International Journal of Unmanned Systems Engineering, Vol. 1, No. 3, pp. 16-47, 2013.

[14] R. Sabatini, M.A. Richardson, C. Bartel, A. Kaharkar, T. Shaid, L. Rodriguez and A. Gardi, "A Low-cost Vision Based Navigation System for Small Size Unmanned Aerial Vehicle Applications", Journal of Aeronautics and Aerospace Engineering, Vol. 2, No. 3, 2013.

[15] S. Ramasamy, R. Sabatini, A. Gardi, Y. Liu, "Novel Flight Management System for Real-Time 4-Dimensional Trajectory Based Operations", in *Proc. of the AIAA Guidance, Navigation & Control (GNC) Conference 2013*, Boston, Massachusetts, USA, 2013.

[16] S. Ramasamy, R. Sabatini, Y. Liu, A. Gardi, L. Rodriguez Salazar. "A Novel Flight Management System for SESAR Intent Based Operations", in *Proc. of the European Navigation Conference 2013 (ENC 2013)*, Vienna, Austria, 2013.

[17] A. Gardi, R. Sabatini, S. Ramasamy, K. de Ridder, "4-Dimensional Trajectory Negotiation and Validation System for the Next Generation Air Traffic Management", in *Proc. of the AIAA Guidance, Navigation & Control (GNC) Conference 2013*, Boston, Massachusetts, USA, 2013.

[18] A. Gardi, R. Sabatini, K. De Ridder, S. Ramasamy. L. Rodriguez Salazar. "Automated Intent Negotiation and Validation System for 4-Dimensional Trajectory Based Operations", in *Proc. of the European Navigation Conference 2013 (ENC 2013)*, Vienna, Austria, 2013.